

1 Validation of a new cavity ring-down spectrometer
2 for measuring tropospheric gaseous hydrogen
3 chloride

4 *Teles C. Furlani¹, Patrick R. Veres², Kathryn E.R. Dawe^{3, a}, J. Andrew Neuman^{2, 4}, Steven S.*
5 *Brown^{2, 5}, Trevor C. VandenBoer¹, Cora J. Young^{1*}*

6 ¹ Department of Chemistry, York University, Toronto, ON, Canada

7 ² NOAA Chemical Sciences Laboratory, Boulder, CO, USA

8 ³ Department of Chemistry, Memorial University of Newfoundland, St. John's, NL, Canada

9 ⁴ Cooperative Institute for Research in Environmental Sciences, University of Colorado, Boulder, CO, USA

10 ⁵ Department of Chemistry, University of Colorado, Boulder, CO, USA

11 ^a Now at SEM Ltd., St. John's, NL, Canada

12 *Correspondence to: youngcj@yorku.ca

13 **Abstract**

14 Reliable, sensitive, and widely available hydrogen chloride (HCl) measurements are important for
15 understanding oxidation in many regions of the troposphere. We configured a commercial HCl
16 cavity ring-down spectrometer (CRDS) for sampling HCl in the ambient atmosphere and
17 developed validation techniques to characterize the measurement uncertainties. The CRDS makes
18 fast, sensitive, and robust measurements of HCl in a high finesse optical cavity coupled to a laser
19 centered at 5739 cm⁻¹. The accuracy was determined to reside between 5–10%, calculated from
20 laboratory and ambient air intercomparisons with annular denuders. The precision and limit of

21 detection (3σ) in the 0.5 Hz measurement were below 6 pptv and 18 pptv, respectively for a 30
22 second integration interval in zero air. The response time of this method is primarily characterized
23 by fitting decay curves to a double exponential equation and is impacted by inlet
24 adsorption/desorption, with these surface effects increasing with RH and decreasing with
25 decreasing HCl mixing ratios. The minimum 90% response time was 10 seconds and the
26 equilibrated response time for the tested inlet was 2–6 minutes under the most and least optimal
27 conditions, respectively. An intercomparison with the EPA compendium method for quantification
28 of acidic atmospheric gases showed good agreement, yielding a linear relationship statistically
29 equivalent to unity (slope of 0.97 ± 0.15). The CRDS from this study can detect HCl at
30 atmospherically relevant mixing ratios, often performing comparable or better in sensitivity,
31 selectivity, and response-time from previously reported HCl detection methods.

32

33 **1. Introduction**

34 Halogenated compounds that participate in catalytic cycles in the atmosphere have major
35 impacts on atmospheric chemistry. Chlorine-containing species have long been known to
36 catalytically destroy stratospheric ozone (Solomon, 1999) and can have similar impacts on
37 tropospheric ozone in polar regions (Simpson et al., 2007, 2015). In particular, early morning
38 oxidation in the troposphere can be influenced heavily by chlorine atoms released by photolabile
39 chlorine species (Osthoff et al., 2008; Thornton et al., 2010; Young et al., 2012, 2014). It is
40 estimated that reactions involving chlorine atoms account for 14–27% of global tropospheric
41 oxidation of abundant volatile organic compounds (VOCs) (Sherwen et al., 2016).

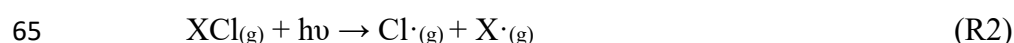
42 The role of chlorine chemistry in the troposphere remains uncertain in part due to a lack of
43 a complete understanding of the contribution of chlorine reservoir species to the tropospheric

44 chlorine inventory (Osthoff et al., 2008; Young et al., 2014). Sources of inorganic chlorine to the
45 troposphere are important because many of them are photochemically active (e.g. ClNO₂). A near-
46 complete budget of inorganic tropospheric chlorine from aircraft transects of polluted North
47 American continental outflow during the WINTER campaign demonstrated that hydrogen chloride
48 (HCl) makes up 48–62 % of total inorganic chlorine, and approximately 98% of total gaseous
49 inorganic chlorine (Haskins et al., 2018). Troposphere HCl levels are typically between 10 and
50 1000 parts per trillion by volume (pptv) (e.g. Crisp et al. (2014); Haskins et al. (2018); and Young
51 et al. (2013)). Elevated levels of HCl are typically found near marine environments polluted with
52 NO_x; where reactions involving the chloride in sea spray aerosols can be a major source of chlorine
53 to the troposphere (Crisp et al., 2014; Finlayson-Pitts et al., 1989; Haskins et al., 2018; Wang et
54 al., 2019).

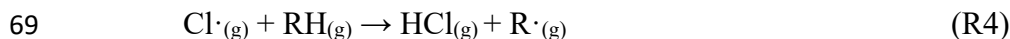
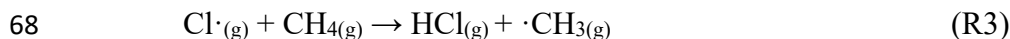
55 HCl is directly emitted to the atmosphere predominantly from volcanic activity, biomass
56 burning, and industrial sources (Butz et al., 2017; Crisp et al., 2014; Keene et al., 1999). HCl is
57 also produced through heterogeneous acid displacement reactions of strong acids, such as nitric
58 acid, with particulate chloride (pCl⁻) (Bondy et al., 2017; Clegg and Brimblecombe, 1985; Gard et
59 al., 1998; Valach, 1967; Wang et al., 2019):



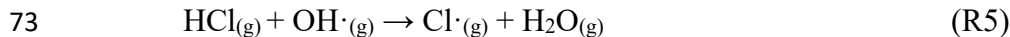
61 where M represents a cation in a chloride salt (often sodium). Elevated levels of chlorine atoms
62 may also be present in both indoor and outdoor environments due to the emission of photolabile
63 reactive chlorine compounds (Dawe et al., 2019; Mattila et al., 2020; Osthoff et al., 2008; Young
64 et al., 2014, 2019).



66 Secondary production of HCl predominantly occurs *via* the reaction of chlorine atoms with
67 methane or VOCs by hydrogen abstraction:



70 The loss of gas-phase HCl occurs predominantly through wet or dry deposition which are terminal
71 sinks for tropospheric chlorine (Wang et al., 2019), with minor loss by reaction with the hydroxyl
72 radical (OH) to re-form chlorine atoms:



74 The balance between loss and formation of chlorine atoms from HCl is highly dependent on factors
75 such as the presence of pCl⁻, NO_x (NO_x=NO+NO₂), and HCl deposition rate (Finlayson-Pitts et
76 al., 1989; Roberts et al., 2008).

77 Measuring HCl in the gas phase is challenging as it readily adsorbs to surfaces. Methods
78 for atmospheric HCl detection must be sensitive, robust, and selective and address HCl interactions
79 with instrument surfaces. Mass spectrometry based measurement techniques have been developed
80 for the detection of HCl in both the stratosphere and troposphere (e.g. Huey et al. (Huey et al.,
81 1996) and Marcy et al. (2004)). Other methods include scrubbing ambient air using an annular
82 denuder and/or a tandem mist chambers to collect HCl, followed by offline analysis such as ion
83 chromatography (IC) (Keene et al., 2007, 2009; United States Environmental Protection Agency,
84 1999; Young et al., 2013). Online detection methods such as chemical ionization time of flight
85 mass spectrometry (CI-ToF-MS) (Crisp et al., 2014), negative ion proton transfer chemical
86 ionization mass spectrometry (NI-PT-CIMS) (Veres et al., 2008), and negative mode atmospheric
87 pressure chemical ionization coupled to triple quadrupole mass spectrometry (APCI-MS-MS)

88 (Karellas et al., 2003) have been shown to be reliable and sensitive methods for HCl detection.
89 Limitations to these existing HCl measurement techniques include some or all of the following;
90 detection limits that are not suitable for the low level of HCl in the troposphere, slow time response,
91 lack of portability, and calibration challenges. Spectroscopic techniques offer distinct advantages
92 over some previous methods. Spectroscopic techniques for measuring atmospheric HCl reported
93 by Hagen et al. (2014) and Wilkerson et al. (2021) have shown the precedent for fast time response,
94 as well as sensitive, selective, and robust detection. The portability and fast time response for
95 instruments is of great importance for spatial resolution and is therefore a key factor for field
96 deployment.

97 Measurements of HCl are typically calibrated using HCl from permeation devices and or
98 standards in compressed gas cylinders. Method validation for HCl measurements are rare, but can
99 reduce these uncertainties (Hagen et al., 2014; Wilkerson et al., 2021). In this paper we
100 demonstrate the versatility and validation of a new commercial cavity ring-down spectrometer
101 (CRDS) for in-situ atmospheric gas phase HCl measurements. First, we compare this CRDS with
102 existing HCl measurement techniques through lab and field intercomparisons. Finally, we describe
103 and characterize surface effects and recommend inlet configurations for best practices when
104 conducting ambient sampling.

105 **2. Materials and experimental methods**

106 **2.1 Chemicals**

107 Reagent grade hydrochloric acid (HCl, 12 M) was used in permeation device construction
108 (see Section 2.3). Potassium hydroxide (KOH) pellets were used to create scrubbing solution for
109 permeation device gas collection. Commercially available reagents were from Sigma-Aldrich
110 (Oakville, Ontario, Canada) and Ultra zero air (grade 5.0) gases were from Praxair (Toronto,

111 Ontario, Canada). Experiments used deionized water generated by a Barnstead Infinity Ultrapure
112 Water System (Thermo Fisher Scientific, Waltham, Massachusetts, USA; $18.2 \text{ M}\Omega \text{ cm}^{-1}$). Annular
113 denuder coating solution was prepared with reagent grade ($>95.5\%$) sodium carbonate (Sigma-
114 Aldrich, St. Louis, Missouri, USA), reagent grade glycerol (Sigma-Aldrich, St. Louis, Missouri,
115 USA), HPLC grade methanol (Fisher Chemicals, Ottawa, Ontario, Canada), and $18.2 \text{ M}\Omega \text{ cm}^{-1}$
116 deionized water. Eluent for annular denuder IC analysis was prepared from sodium hydroxide
117 solution (NaOH, 50% w/w, Thermo Fisher Scientific, Sunnyvale, California, USA). IC calibration
118 standards were prepared through serial dilution of a mixed anion standard concentrate (Thermo
119 Fisher Scientific, Dionex Seven-Anion II, P/N: 057590). Nitrogen (grade 4.8).

120 **2.2. Cavity ring-down spectrometer (CRDS)**

121 The Picarro G2108 Hydrogen Chloride Gas Analyzer system was used for all analyses.
122 The basic operating principles of this CRDS are similar to analogous Picarro greenhouse gas
123 instruments that have been described in detail by Crosson et. al (2008). The CRDS consists of a
124 tunable laser, a wavelength monitor, and a heated optical cavity ($80 \text{ }^\circ\text{C}$). All the components of
125 this analyzer and internal stainless-steel fittings are contained within a heat-regulated metal case
126 maintained at $45 \text{ }^\circ\text{C}$. The laser radiation (1742 nm , 5739 cm^{-1}) is directed by a fiber optic cable to
127 the wavelength monitor and optical cavity. The first overtone (2-0 absorption band) of HCl is
128 easily discernable from other absorbing species (e.g. H_2O , CH_4), has a relatively high intensity
129 compared to the fundamental absorption transition, and is accessible to near-infrared (IR) diode
130 laser light sources. The optical cavity is fitted with three highly reflective dielectric-coated fused
131 silica mirrors ($R > 99.995\%$, ring down time constant of $53 \text{ }\mu\text{sec}$, equivalent to a path length of 16
132 km) oriented in an acute triangular arrangement supported by an invar housing. The reflectivity of
133 the mirrors is measured from the laser signal loss in an analyte-free optical cavity under inert gas

134 flow. The CRDS flow rate is 2 L min⁻¹ and the cavity is held at a reduced pressure of 18.70 ± 0.02
135 kPa (140 Torr) thermostated to 80.000 ± 0.005°C. One mirror is mounted on a piezoelectric
136 actuator to achieve optical resonance between the laser frequency and the longitudinal modes of
137 the cavity. The laser is shut off rapidly (< 1 μsec) once resonance is achieved. A photodetector
138 monitors the decay of the photons exiting the cavity through another mirror. Custom electronics
139 digitize the signal for fitting of an exponential decay; the time constant of the decay, τ, is converted
140 to absorbance, α, using the expression

$$141 \quad \alpha = 1 / c\tau - 1 / c\tau_0 \quad E1$$

142 where c is the speed of light. The instrument measures 30 specific frequencies within ~1 cm⁻¹
143 centered at 5739 cm⁻¹ to fit the absorption spectra of trace species in this region (see Figure S2).
144 HCl, H₂O, and CH₄ mixing ratios are reported every 2 seconds, though the true time response of
145 the measurement method is limited by surface effects (see Section 3.4). Gaseous inorganic chlorine
146 reservoir species (e.g. ClNO₂) cannot thermally dissociated under the cavity (80 °C) conditions
147 (Thaler et al., 2011). The instrument zero measurement drift is reduced by a high precision
148 distributed feedback laser centered at 5739.2625 cm⁻¹ coupled with a custom-designed wavelength
149 monitor to determine the frequency axis of each spectrogram. To mitigate particulate matter optical
150 extinction and surface deposition on the high reflectivity mirrors, two high efficiency particulate
151 air (HEPA) filters are placed upstream of the cavity, contained within the 45 °C heat-regulated
152 compartment.

153 **2.3 In-house HCl permeation device validation**

154 The in-house assembly of HCl permeation devices (PDs) is described in detail in Lao et al.
155 (2020). Briefly, 200 μL of 12 M aqueous HCl solution was pipetted into a 7.62 cm perfluoroalkoxy
156 (PFA) tube (3 mm i.d. with 1 mm thickness) plugged at both ends with porous

157 polytetrafluoroethylene (PTFE) (1 cm length by 3.17 mm o.d.). The polymers allow a consistent
158 mass of HCl to permeate at a given temperature and pressure. An aluminum block that was
159 temperature-controlled using a cartridge heater (OmegaTM; CIR-2081/120V, Saint-Eustache, QC,
160 Canada) housed the PD and was regulated to 60.0 ± 0.1 °C by a process controller. Dry N₂ flowed
161 through a PFA tube (1.27 cm o.d.) in the block, containing the PD. Stable flows of 49 ± 2 standard
162 cubic centimeters per minute (sccm) through the oven were maintained with a 50 μm diameter
163 critical orifice (Lenox laser, Glen Arm, Maryland, USA, 15 psi; SS-4-VCR-2-50). Flows were
164 measured using a DryCal Definer 220 (Mesa Labs, Lakewood, Colorado, USA). The mass
165 emission rate of HCl from the PD was quantified by scrubbing into a 25 mL glass impinger
166 containing 1 mM KOH over 24 h followed by analysis using IC with conductivity detection (CD).
167 Mass emission rates for the PD were determined as 140 ± 18 ng min⁻¹ (n=3, ± 1σ) at 60 °C.

168 **2.4 Laboratory intercomparison**

169 A laboratory intercomparison between the CRDS and offline-measured HCl scrubbed into
170 a basic solution of 100 mM KOH by delivering gaseous HCl from the permeation device to the
171 sampling systems. The 140 ng min⁻¹ of HCl in dry N₂ from the PD was mixed into a zero air
172 dilution flow of 2.1 to 8.0 L min⁻¹, to provide standard addition HCl mixing ratios that ranged from
173 12 to 45 ppbv.

174 The dilution flow was maintained using a 10 L min⁻¹ mass flow controller (GM50A, MKS
175 instruments, Andover, Massachusetts, USA). All inlet lines and fittings were kept at ambient
176 temperature (~25 °C) and were made of PFA unless stated otherwise. The inlet mixing line
177 between the PD emissions and the humidified dilution flow was 3.17 mm i.d. and 45 cm in length.
178 Residence times for HCl in the sampling line ranged from 0.02 to 0.08 seconds. To vary relative
179 humidity (RH), a controlled flow of zero air was directed into a glass impinger at room temperature

180 containing deionized water to yield a water-saturated air stream. The humidified flow was passed
181 through a 2 μm Teflon filter (TISCH scientific, North Bend, Ohio, USA) in a PFA holder to
182 prevent any aqueous droplets from entering the experimental lines. The RH was set by mixing
183 with dry zero air to generate 0, 20, 50, and 80 % RH values.

184 **2.5 Ambient intercomparison**

185 An ambient intercomparison was undertaken by measuring outdoor air with the CRDS in
186 parallel with sodium carbonate-coated annular denuders. A total of 11 denuder samples were
187 collected alongside continuous CRDS observations, each for approximately 24 hours between 4–
188 11 April 2019. The measurement site was the Air Quality Research Station, located on the roof of
189 the Petrie Science and Engineering Building at York University in Toronto, Ontario, Canada
190 (43.7738° N, 79.5071° W, 220 m above sea level). All indoor inlet lines and fittings were kept at
191 room temperature while the outdoor temperature ranged from -2 to 14 °C. All inlet lines and
192 fittings were made of PFA unless stated otherwise. A full schematic of the sampling apparatus
193 indicating the separation between the outdoor and indoor inlet positions is provided in Figure S5.
194 A 22 L min^{-1} sampling flow was pulled through a URG Teflon Coated Aluminum Cyclone (URG
195 Corporation, Chapel Hill, North Carolina, USA) with a 2.5 μm cut-off for particulate matter. The
196 inlet lines were such that each sampling setup collected HCl at equal residence time to ensure
197 equivalent wall losses of HCl. The shared inlet line was 4.65 m in length and had an i.d. of 4.76
198 mm. The flow was split between the 1.5 m denuder sampling line (20 L min^{-1}) and the 0.15 m
199 CRDS sampling line (2 L min^{-1}), yielding a 0.375 sec residence time for both methods. The
200 denuder line flow was equally divided into two multichannel etched glass annular denuders (URG
201 Corporation, Chapel Hill, North Carolina, USA, 4 channel, 242 mm length, URG-2000-30x242-
202 4CSS) at 10 L min^{-1} . The denuders collected HCl in parallel to each other with flows controlled

203 using two separate 10 L min⁻¹ mass flow controllers (GM50A, MKS instruments). Denuders were
204 coated with a solution of 2% w/w sodium carbonate and 0.1% w/w glycerol in a solution of 1:1
205 methanol:water. A 15 mL aliquot of coating solution was dispensed into a denuder and two
206 polypropylene caps affixed. The sealed denuders were inverted and rotated for a few minutes to
207 ensure an even coating. The excess coating solution was decanted, and the denuder was dried for
208 15 min with 2 L min⁻¹ of zero air. After sampling, denuders were extracted with 2 aliquots of 5.00
209 mL deionized water, following the same sealing and inversion procedure, for a total extraction
210 volume of 10.00 mL. Extracts were collected into a 15 mL polypropylene tube for storage at 4 °C
211 until analysis. Instances of flagged instrument errors in the CRDS data during ambient
212 observations were removed as standard practice in quality control procedures (see Figure S3). The
213 loss of observational data during such periods corresponds to a negative bias. The CRDS data loss
214 during a given denuder sampling period was included in setting the overall measurement error
215 when intercomparing measurements. The dataset can be found in Furlani et al. (2021).

216 **2.6 Ion chromatography analysis**

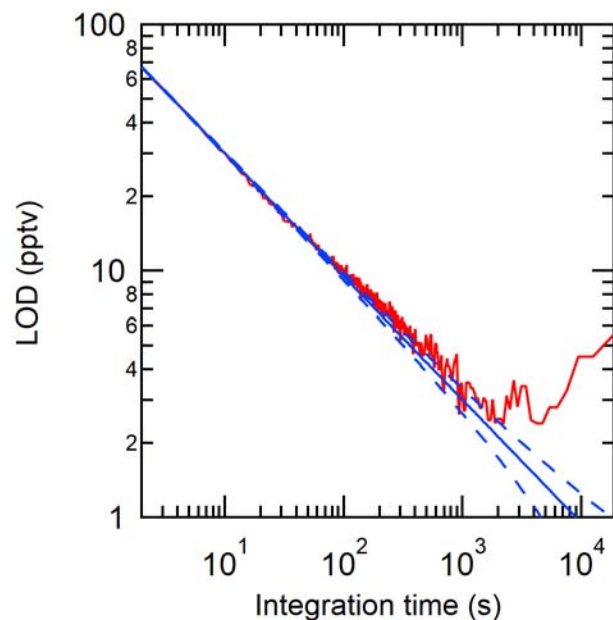
217 Samples collected into an impinger from the HCl PD were analyzed as the chloride anion
218 by IC-CD using an ICS-2100 (Thermo Fisher Scientific, Sunnyvale, California, USA) according
219 to the method described in Place et al. (Place et al., 2018). Annular denuder extracts were analyzed
220 by IC-CD using an ICS-6000 (Thermo Fisher Scientific, Sunnyvale, California, USA). Details of
221 both separation methods can be found in the SI. Chloride was quantified using external calibration
222 with a 5-point calibration curve. Two check standards, located at the high and low ends of the
223 working range, were used to evaluate the accuracy of quantification.

224 **3. Results and discussion**

225 **3.1 Suitability for atmospheric measurements**

226 The selectivity of this CRDS analyzer arises from monitoring a high-intensity spectral line
227 (5739.2625 cm^{-1}). The absorption used by this instrument is suitable for HCl measurements in the
228 ambient atmosphere because abundant atmospheric gaseous species such as CO, CO₂, NO_x, and
229 N₂O (Gordon et al., 2017; Kochanov et al., 2019) do not have major absorption features in the
230 same region. Absorption features of H₂O and CH₄ in this spectral region are part of the fitting
231 parameters used to determine number densities of HCl, as described in Section 2.2. Most organic
232 and inorganic compounds commonly found at trace levels in the atmosphere do not absorb strongly
233 in this region (Gordon et al., 2017; Kochanov et al., 2019). For these compounds to interfere with
234 the CRDS measurement, their mixing ratios would need to be very high (>10s of parts per million
235 by volume, ppmv). Under conditions where the peak shape is compromised by the presence of
236 interfering absorbing species or instrument instabilities (e.g. cavity pressure fluctuations), the
237 instrument fitting is interrupted and the “bad” data is flagged, thereby allowing simple quality
238 control (see Figure S3).

239 The limit of detection (LOD) of the CRDS analyzer is suitable for expected HCl levels in
240 the atmosphere. Instrument LODs were calculated as three times the Allan-Werle deviation (Figure
241 1, Hagen et al., 2014) when overflowing a 15 cm inlet (3.17 mm i.d.) with zero air directed into
242 the CRDS for ~10 hours. The LODs determined in the CRDS measurements for 2 second, 30
243 second, 5 minute, and 1 hour integration times were 66, 18, 5, and 2 pptv, respectively. Similarly,
244 precision was determined from the Allan-Werle deviation in the blank over the same 10 hours of
245 zero air sampling. Precision in a 2 second, 30 second, 5 minute, and 1 hour integration time was
246 22, 6, 2, and 0.8 pptv, respectively.



247
 248 **Figure 1.** Allan-Werle deviation (3σ) in the optical cavity purged with zero-air (red line) shown with the
 249 ideal deviation (no drift, solid blue line) and associated error in the deviation (dashed blue line).

250 **3.2 Instrument performance**

251 This CRDS has many advantages compared to methods previously used to measure HCl in
 252 the ambient atmosphere (Table 1). The LOD and precision of the instrument is comparable to prior
 253 high time-resolution methods, allowing changes in HCl mixing ratio of a few pptv to be measured.
 254 The accuracy/uncertainty is the hardest to compare due to the differences in assessment. A
 255 particular challenge is that other methods require external calibrations to determine accuracy and
 256 a stable, accurately calibrated HCl source at atmospherically relevant mixing ratios is challenging
 257 to obtain (Lao et al., 2020; MacInnis et al., 2016). In contrast, spectroscopic techniques offer a
 258 distinct advantage as they are absolute measurements and accuracy determinations rely on
 259 propagating uncertainty in the measured parameters (i.e. wavelength and the time constant τ). In
 260 the absence of determining accuracy of the CRDS from its operating parameters we use the
 261 deviations in our intercomparisons to estimate the accuracy of the full system, i.e. the instrument
 262 and ambient sampling inlet combined. We assess the total method uncertainty using

263 intercomparisons with the gold standard for atmospheric acid detection (EPA Compendium
 264 method IO-4.2, United States Environmental Protection Agency (United States Environmental
 265 Protection Agency, 1999)) due to the greater uncertainty when considering the potential total
 266 system error from the sorption/desorption to all sampling surfaces (i.e., instrument and inlet). We
 267 measured that the accuracy of the analyzer ranges from 5 to 15%. This is a conservative range
 268 based on the methods we used to validate the instrument, which is further described in Section 3.3.
 269 The response time of the CRDS used in this work is fast compared to most measurements; the
 270 limitation for all online-line methods compared in Table 1 is not the measurement frequency, but
 271 rather the time required for HCl to adsorb and desorb from the inlet to the sample stream, which
 272 is discussed further in Section 3.5. Lastly, instrument size and power consumption of this CRDS
 273 are much lower than many other techniques and are major advantages when considering use in the
 274 field, particularly for mobile platforms.

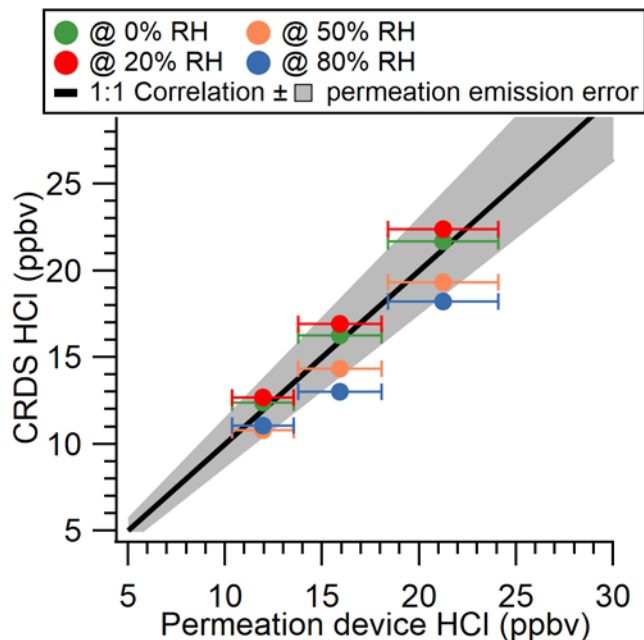
275 **Table 1.** Performance characteristics of CRDS HCl analyzer compared to previously reported
 276 methods.

Instrument	LOD	Accuracy/ Uncertainty	Precision	Measurement frequency	Instrument Size	Power Consumption	Reference
<i>Near-IR CRDS</i>	<18 pptv ^a (30 sec)	5–15%	6 pptv (30 sec)	2 s ^e	31.75 kg 43.2 x 17.9 x 44.6 cm	110 W (analyzer) 75 W (pump)	This study
<i>Near-IR CRDS</i>	60 pptv ^a (1 min)	<10%	20 pptv (1 min)	<15 s	NR	NR	(Hagen et al., 2014)
<i>Off-axis integrated cavity output spectrometer (OA-ICOS)</i>	78 pptv (30 sec)	<11%	26 pptv (30 sec)	1 s	NR	NR	(Wilkerson et al., 2021)
<i>Aircraft laser infrared absorption spectrometer</i>	33 pptv ^b	10 %	0.1 ppbv (30 sec)	<30 s	72 kg	NR	(Voss et al., 2001; Webster et al., 1994)

<i>Quartz-enhanced photoacoustic spectroscopy (QEPAS)</i>	550 pptv ^a	NR	526 ppbv	NR	NR	NR	(Ma et al., 2016)
<i>Acetate CI-ToF-MS</i>	97 pptv ^a	30%	32.3 pptv	<1 s	59 x 42 x 83 cm	<2000 W peak	(Crisp et al., 2014)
<i>Iodide CI-HR-ToF-MS</i>	30 pptv ^a (30 sec)	30%	10 pptv (30 sec)	0.22 s	~ 59 x 42 x 83 cm	<2000 W peak	(Lee et al., 2018)
<i>Sulfur pentafluoride ion trap CIMS</i>	66 pptv ^a	10%	22 pptv	1.6 s	NR	NR	(Jurkat et al., 2010)
<i>APCI-MS-MS</i>	335 pptv ^a	NR	NR	5 s	NR	< 17.5 kW	(Karellas et al., 2003)
<i>Tandem mist chamber and IC-CD</i>	48 pptv ^c	<25 %	24 pptv ^c	2 h	NR	NR	(Keene et al., 2007, 2009)
<i>Annular denuder and IC-CD</i>	6.9–42 pptv ^d	10%	NR	Hours–Days	>10 kg	400 W (Sampling equipment only)	This study

277 a: 3σ , b: predicted assuming a minimum detectable line-center absorption of 1×10^{-5} can be achieved in 30 s, c:
278 precision (σ) determined from averaged paired measurements in 2 h samples on IC-CD and LOD was calculated at
279 2σ , d: 3σ calculated range for a 24-hour sampling time from three denuder method blanks, e: instrument data reporting
280 frequency. The true measurement frequency will also be affected by surface effects, as described in section 3.4, and
281 NR: not reported.

282 3.3 Laboratory and ambient intercomparison

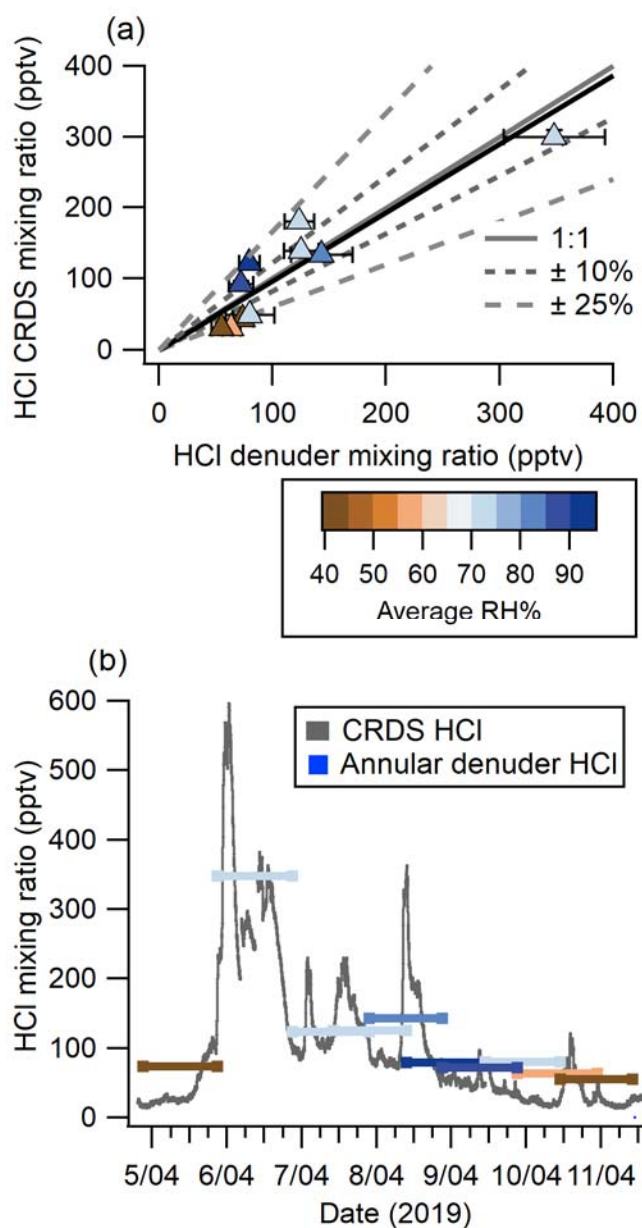


283

284 **Figure 2.** Comparison of CRDS HCl measurements and output from an HCl permeation device over a
 285 range of RHs. Error bars in the x direction represent propagated IC measurement error, while error bars in
 286 the y direction represent the standard deviation of online sampling plateau for each mixing ratio (low
 287 magnitudes mean these error bars do not extend beyond the points). A 1:1 correlation (solid black line) is
 288 shown with the uncertainty in the permeation device emission rate (shaded grey area).

289 We compared the CRDS analyzer-measured HCl with the gas standard mixing ratios
 290 provided by an IC-certified PD under dry conditions and observed a close to 1:1 correlation. We
 291 explored 5 mixing ratios 12, 16, 21, 32, and 45 ppbv. These levels are higher than have been
 292 observed in the ambient atmosphere but demonstrate good single response linearity. When the HCl
 293 gas entrained in flows of higher RH ($\geq 50\%$) a negative bias was observed, although the
 294 measurements generally remained within the quantified error in the PD output. Negative bias from
 295 the provided HCl mixing ratios at 50% and 80% RH were 9.6% and 14.9%, respectively. As
 296 described above, there is no spectroscopic water absorption interference in the HCl measurement
 297 indicating that water increased HCl losses to gas handling surfaces for experiments conducted in
 298 humidified air. Inlet surface effects are well established for gaseous strong acids and bases, as
 299 these compounds readily sorb at interfaces (e.g. Eisele and Tanner (1993), Kim et al. (2008),

300 Neuman et al. (1999), Pszenny et al. (1993), Roscioli et al. (2016)). The comparison presented
301 here is a best-case scenario because the sampled mixing ratios were much greater than expected in
302 the ambient atmosphere, and therefore less likely to be impacted by surface effects. Surface effects
303 under humid conditions necessitated the mitigation and quantification efforts described further in
304 Section 3.5. To practically validate the CRDS under real-world conditions, an ambient
305 intercomparison was performed over a period of 7 days (4–11 April 2019).



306

307 **Figure 3.** (a) Comparison of HCl measured 4–11 April 2019 using annular denuders and CRDS (averaged
308 to the collection time of denuders). Denuder error bars are derived from the error in the IC calibration,
309 standard deviation of method blanks, and extraction recovery. CRDS measurement errors are the precision
310 in a single measurement combined with data loss for flagged instrument errors. Also shown are a 1:1
311 correlation line (solid grey), 10 % (short grey dash) and 25 % (long grey dash) deviation from 1:1, and the
312 orthogonal distance regression (solid black). Points are coloured by the average RH during sampling. (b)
313 Continuous HCl mixing ratio timeseries by CRDS overlaid with averaged 24-hour denuder measurement
314 analyzed by IC with lines coloured according to the average RH during sampling.

315

316 Online HCl detection by CRDS showed good agreement with HCl mixing ratios quantified
317 from ten annular denuder extracts collected according to EPA Compendium method IO-4.2
318 (United States Environmental Protection Agency, 1999), which is a standard offline method for
319 quantitation of acidic atmospheric gases (see Figure 3a). Measurements from the 2 instruments
320 were linearly related with a slope of 0.97 ± 0.15 , as determined by orthogonal least distance
321 regression, with a y-intercept of -0.001 ± 0.021 . Half of the measurements are within 10 % of a
322 1:1 correlation and the remaining half fall within 25 %. To further validate the comparison a linear
323 correlation coefficient (see Figure S7) of 0.93 ± 0.14 was determined for the two methods and
324 shows good agreement with the orthogonal least distance regression. Changes in RH had no
325 systematic bias on the correlation. Our intercomparison indicates that CRDS measures HCl with
326 comparable results to those obtained by carbonate-coated annular denuders. While the latter
327 requires offline analysis, the CRDS has the additional benefit of continuous high time resolution
328 measurements at 0.5 Hz and dramatically better precision.

329 Although average HCl measurements between the CRDS and denuders agreed well, much
330 of the useful temporal variability were lost in the time-integrated denuder data (see Figure 3b). For
331 example, from 19:00 April 5 to 01:00 April 6 the CRDS measured mixing ratios between 91 and

332 598 pptv. This rapid change of mixing ratios is not captured by the 24-hour average denuder-
333 measured mixing ratio of 348 pptv. The fast time response of the CRDS also captured other rapidly
334 changing HCl features such as the peak observed on between 00:00–06:00 on April 7. The 6-hour
335 event started at 80 pptv and increased at a rate of $1.2 \text{ pptv min}^{-1}$ to 230 pptv over ~ 120 minutes,
336 followed by a decrease at a rate of $0.5 \text{ pptv min}^{-1}$ for ~ 240 minutes to 98 pptv. The fast time
337 response of the CRDS on the order of minutes is crucial when applying the technique to the real
338 atmosphere for the purpose of fully constraining the sources and sinks for HCl, for which many
339 precursors have similar lifetimes, and ultimately improve our understanding of the Cl budget
340 (Crisp et al., 2014).

341 Results from the laboratory and ambient intercomparisons were used to determine the
342 accuracy of the HCl analyzer as 5 to 15 %. The lower bound of uncertainty (5 %) was determined
343 from the laboratory intercomparison under the optimal dry conditions (Figure 2). The upper bound
344 of uncertainty (15 %) was consistent across the laboratory intercomparison under the highest RH
345 (80%) conditions tested (Figure 2) and the standard deviation of the orthogonal distance regression
346 slope from the ambient intercomparison (Figure 3a).

347 **3.4 Sampling line and instrument response time assessment**

348 We have thus far demonstrated the efficacy of the CRDS for accurately analyzing gas
349 standards and ambient HCl. However, the potential for sampling losses or desorption sources of
350 surface-active gases that could affect the quality of such measurements is ubiquitous, and the study
351 of these effects are well established (Crisp et al., 2014; Ellis et al., 2010; Pollack et al., 2019;
352 Roscioli et al., 2016). This makes quantification a challenge as there are typically long
353 equilibration times associated with signal stabilization. Long equilibrations make fast time
354 response detection difficult without first characterizing line sorption and desorption, followed by

355 making inlet modifications to minimize losses (Deming et al., 2019; Ellis et al., 2010; Pagonis et
356 al., 2017). To ensure accurate field measurements of HCl, a characterization of the magnitude of
357 HCl loss and desorption during sampling was made. The response time of an instrument to a rapid
358 change in HCl can be calculated by both the time it takes for the measurement to go from zero to
359 100 % of the HCl quantity being delivered, as well as the time it takes to return from the HCl
360 quantity being delivered back to zero.

361 Inlet and instrument surface effects for surface active gases such as HCl can be
362 characterized by fitting decay curves to a double exponential (Ellis et al., 2010; Moravek et al.,
363 2019; Pollack et al., 2019; Zahniser et al., 1995);

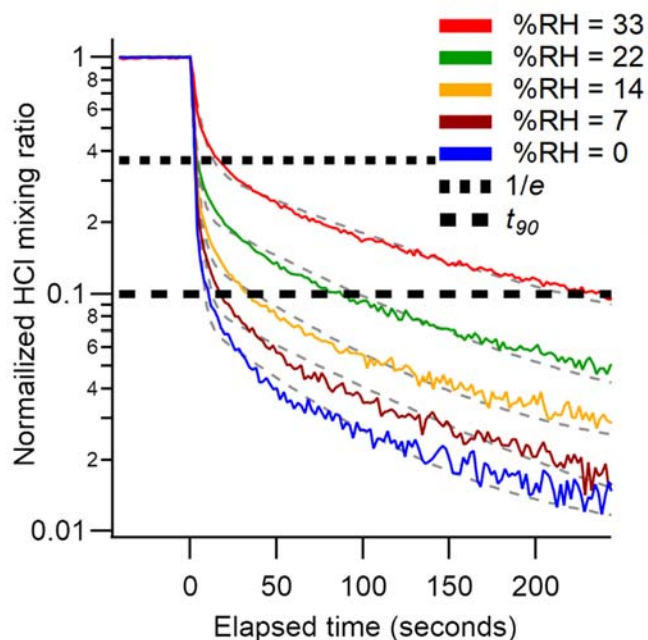
$$364 \quad y = y_0 + A_1 e^{\left(\frac{-t-t_0}{\tau_1}\right)} + A_2 e^{\left(\frac{-t-t_0}{\tau_2}\right)} \quad \text{E2}$$

365
366 Where y is the mixing ratio of HCl, y_0 is the mixing ratio at the end of the decay, A_1 and A_2 are
367 proportionality coefficients that determine how much the decay is governed by τ_1 and τ_2
368 respectively, t is the time elapsed, and t_0 is the initial time. The first time constant (τ_1) represents
369 air exchange within the instrument, while the second (τ_2) is the surface interaction equilibrium
370 time between HCl adsorbed to surfaces and the overlying airstream mixing ratio. The only term in
371 this equation that can be optimized for the CRDS is τ_2 , which can be reduced by decreasing the
372 amount of time HCl interacts with inlet surfaces. The sampling flow rate and cavity temperatures
373 are constant for the commercial software and not adjustable, therefore changing the value of τ_1
374 was not explored in this study. In most reports τ_1 represents the largest change in signal and
375 represents instrument response time. For example, Whitehead et al. (2008) found that τ_1 values
376 governed >75% (i.e. A_1) of changes in measured NH_3 . For the CRDS, measured values of τ_1 were

377 between 5 and 10 seconds under all conditions and could be improved with a faster inlet flowrate
378 for the CRDS to subsample from.

379 An additional set of experiments was undertaken in which a 24 ppbv HCl standard was
380 sampled while varying RH from 0 to 33% (Figure 4). The effect of RH on the response time of the
381 CRDS was measured using a method similar to that described in Section 2.4. The HCl standard
382 gas was sampled over three 10 min pulses at each RH ($\pm 2\%$). The HCl standard was introduced
383 into a 3.17 mm i.d. PFA tube and 10 cm long inlet line. Data was background corrected to levels
384 measured prior to the standard addition and the signal was normalized to the HCl enhancement
385 during the final 10 seconds of each HCl pulse. Due to a lack of inlet characterization for systems
386 measuring HCl, we compare our decay constants to literature values for compounds with similar
387 surface-active properties (e.g. HNO₃ and NH₃). The instrument exchange rate (τ_1) values for
388 spectroscopic methods measuring HNO₃ and NH₃ are generally faster than our measured values
389 for HCl. However, it should be noted that measurements of τ_1 reflect differences in sampling flow
390 rates and internal volume and are likely affected by the internal filters present in the HCl CRDS.
391 Typically, τ_1 was <2 seconds (Ellis et al., 2010; Pollack et al., 2019; Roscioli et al., 2016), but
392 could be as high as 4.5 seconds for larger pulses (1 ppmv) of analyte (Roscioli et al., 2016). We
393 observed a highly variable surface interaction equilibrium time constant (τ_2), with values ranging
394 between 97 and 350 seconds. Reported values of τ_2 for other surface-active gases are similarly
395 variable, with values <50 seconds for heated short clean inlets (Ellis et al., 2010; Pollack et al.,
396 2019; Roscioli et al., 2016), and ~300 seconds for a contaminated inlet measuring NH₃ (Pollack et
397 al., 2019). Major differences in the surface area between our instrument and the instruments to
398 which we compare are likely to cause τ_2 differences. Our method employs the use of three filters

399 that increase the gas to surface interactions, and therefore increase our equilibrated response time
400 τ_2 .



401
402 **Figure 4.** Background corrected and normalized signal decay curves observed for pulsed HCl (24 ppbv)
403 performed at various RHs. Dashed grey lines represent a double exponential fit to the average of three
404 cycles at each water mixing ratio. The short and long dashed black lines indicate 37 % ($1/e$) and 90 % (t_{90})
405 decrease from the initial signal, respectively.
406

407 Another method for quantifying response time is by calculating the e-folding ($1/e$) signal
408 loss with respect to time. Calculated e-folding response times demonstrated the fast exchange
409 within the system with values comparable to τ_1 . Similarly, a signal decrease of 90% (t_{90}) illustrates
410 the total decay of the sampling line. Using e-folding response time and t_{90} offers a better visual
411 understanding of the relative roles for instrument and inlet responses and the impacts of increasing
412 RH. We summarize the double exponential decay constants, e-folding response time, and t_{90} for
413 the rise and decay of HCl mixing ratios from pulses delivered to the instrument in Table 2 and SI
414 tables 1–4. Increasing the RH increases the response time of the inlet (Figure 4). At the highest
415 experimental RH (33 %), τ_2 is increased by almost a factor of two compared to dry conditions,

416 from seconds to minutes. At lower mixing ratios the higher RH increased the response times to a
417 greater extent (Table 2 and Tables S1–S4). The increased response time at high ambient RH would
418 not compromise stationary measurements in which HCl mixing ratios changed on time scales of
419 minutes to hours but would not capture more rapid changes. The largest impact on CRDS time
420 response likely comes from unavoidable effects of partitioning on the large surface area of the
421 HEPA filters located before the optical cavity. Minimizing inlet effects for the CRDS where
422 observation of HCl mixing ratio changes over <1 min is required (e.g. aircraft or mobile
423 measurements) are most important. The wall interactions of HCl can be reduced by increasing the
424 inlet flow rate and/or decreasing the tubing length (Pagonis et al., 2017).

425 Physical approaches to improving inlet response include inlet material substitution,
426 heating, and pressure reduction, to reduce adsorption of surface-active analytes through removal
427 of surface water and promoted mass transfer of analytes to the gas phase (Sintermann et al., 2011).
428 Deming et. al. (Deming et al., 2019) found that PFA tubing had the lowest delay times for
429 semivolatile compounds and would likely extend to small polar molecules like HCl. For a clean
430 thermally-equilibrated inlet, HCl artifacts can be minimized, but if semivolatile aerosol chloride is
431 sampled (e.g. NH_4Cl), the thermodynamic equilibrium can be shifted to result in a positive bias in
432 the HCl measurement, equivalent to similar considerations when measuring HNO_3 and NH_3 (Ellis
433 et al., 2010; Sintermann et al., 2011; Whitehead et al., 2008). While HEPA filters prevent aerosol
434 from entering the cavity, their elevated temperature (45 °C) could lead to volatilization bias and
435 therefore the use of an inlet filter held at ambient temperature to reduce such effects is
436 recommended at a minimum.

437 Chemical approaches can also help mitigate adsorption of surface-active molecules to inlet
438 surfaces through derivatization or passivation. The silanization of glass or stainless-steel to form

439 an inert fluorinated or silicon coating on a virtual impactor or the introduction of a gaseous
440 fluorinated compound that adsorbs competitively to instrument surfaces in place of the analytes
441 have been demonstrated to substantially reduce surface adsorption on PFA (Ellis et al., 2010;
442 Moravek et al., 2019; Pollack et al., 2019; Roscioli et al., 2016; Wilkerson et al., 2021). However,
443 environmental impacts must be considered when constantly adding fluorinated compounds to
444 sampling flows as they may have deleterious environmental consequences (Cousins et al., 2020).
445 In particular, perfluorobutanesulfonic acid, the fluorinated chemical suggested for passivating
446 inlets (Roscioli et al., 2016), is subject to usage restrictions in some European countries (ECHA,
447 2020) based on potential negative human and environmental health impacts (Benskin et al., 2012;
448 Sunderland et al., 2019). The high surface activity of perfluorobutanesulfonic acid is likely to cause
449 issues in the analyzer used in this work because the gas sample comes into direct contact with the
450 high reflectivity mirrors. Acid deposition onto mirrors will degrade their reflectivity. Silicon
451 coatings on all plumbed surfaces have been successfully used for atmospheric HCl measurements
452 (Wilkerson et al., 2021), and recommended for applications where PFA use is impractical.
453 Although a direct comparison has not been conducted for HCl, PFA inlet material has been
454 reported to yield better response times than silicon coatings for nitric acid (Neuman et al., 1999).
455 Differences in instrument configurations and applications may warrant the use of different inlet
456 materials and coatings for successful measurement of atmospheric HCl.

457 **Table 2.** Summary of the fit parameters for the double exponential decay curves as a
458 function of mixing ratio and humidity, e-folding response time, and t_{90} .

459

Mixing ratio (ppbv)	Residence time (seconds)	RH (%)	τ_1 (seconds)	τ_2 (seconds)	$1/e$ (seconds)	t_{90} (seconds)
12	0.021	0	10.3	123	26.5	101
16	0.028	0	9.6	200	24.7	82
21	0.037	0	10.1	300	26.4	74
24	–	0	2.7	97	2.5	10

		7	5.0	124	2.5	18
		14	5.0	114	2.5	32
		22	5.0	123	3.9	86
		33	10.0	189	16.1	239
32	0.056	0	9.4	188	24.5	62
45	0.079	0	9.7	350	25.6	54

460

461

462 4. Conclusions

463 The suitability of a CRDS analyzer for measuring ambient atmospheric HCl were explored
464 through laboratory and ambient air intercomparisons, assessing their inlet and analyzer sampling
465 challenges to established atmospheric sampling techniques for strong acids. In comparison to other
466 reported instrumentation, the CRDS is shown performing similar or better than the most sensitive
467 HCl measurements reported. As with many in situ measurements of HCl, the most significant
468 limitation is adsorption/desorption loss and release on inlet surfaces, with the deposition effects
469 increasing with increasing RH and decreasing HCl mixing ratios. Given the longstanding
470 knowledge of these issues for surface active gases, such as HNO₃ and NH₃, there are a variety of
471 chemical and physical options, discussed in this study, to mitigate inlet effects and achieve faster
472 response times for the CRDS. Increasing the flowrate of the sampling inlet, while maintaining
473 laminar flow, is the simplest approach to reducing surface effects discussed in Section 3.4. Spectra
474 capturing errors in the measurement of HCl for the CRDS can occur at high levels of VOCs (e.g.
475 near emission point sources or biomass burning plumes) or instrument instabilities (e.g. pressure
476 fluctuations), however potential instrument errors are minimal under most operating and
477 atmospheric conditions. Finally, comparison with annular denuder observations agreed within the
478 combined uncertainties, with the CRDS measurement rate demonstrating the power of capturing
479 transient events that are important to constraining atmospheric chlorine chemistry (e.g. photolysis
480 of precursors, thermodynamic partitioning, and direct emissions).

481 **Acknowledgements**

482 We acknowledge the Natural Sciences Engineering and Research Council of Canada and York
483 University for funding. We thank Andrea Angelucci and Sonya Daljeet for assistance with data
484 collection.

485 **Data availability**

486 The ambient intercomparison dataset can be found in Furlani et al. (2021).

487 **Author contributions**

488 TCF, PRV, and KERD collected and analyzed the data. TCF, PRV, JAN, SSB, TCV, and CJY
489 conceived of and designed the experiments. Funding was obtained by CJY. The manuscript was
490 written by TCF with input from all authors.

491 **Competing interests**

492 The authors declare no competing interests.

493 **References**

- 494 Benskin, J. P., Muir, D. C. G., Scott, B. F., Spencer, C., De Silva, A. O., Kylin, H., Martin, J. W.,
495 Morris, A., Lohmann, R., Tomy, G., Rosenberg, B., Taniyasu, S. and Yamashita, N.:
496 Perfluoroalkyl Acids in the Atlantic and Canadian Arctic Oceans, *Environ Sci Technol*, 46(11),
497 5815–5823, doi:10.1021/es300578x, 2012.
- 498 Bondy, A. L., Wang, B., Laskin, A., Craig, R. L., Nhliziyo, M. V, Bertman, S. B., Pratt, K. A.,
499 Shepson, P. B. and Ault, A. P.: Inland Sea Spray Aerosol Transport and Incomplete Chloride
500 Depletion: Varying Degrees of Reactive Processing Observed during SOAS, *Environ Sci*
501 *Technol*, (51), 9533–9542, doi:10.1021/acs.est.7b02085, 2017.
- 502 Butz, A., Dinger, A. S., Bobrowski, N., Kostinek, J., Fieber, L., Fischerkeller, C., Giuffrida, G.
503 B., Hase, F., Klappenbach, F., Kuhn, J., Lübcke, P., Tirpitz, L. and Tu, Q.: Remote sensing of
504 volcanic CO₂, HF, HCl, SO₂, and BrO in the downwind plume of Mt. Etna, *Atmos Meas Tech*,
505 10(1), 1–14, doi:10.5194/amt-10-1-2017, 2017.

506 Clegg, S. L. and Brimblecombe, P.: Potential degassing of hydrogen chloride from acidified
507 sodium chloride droplets, *Atmos Environ*, 19(3), 465–470, doi:[https://doi.org/10.1016/0004-](https://doi.org/10.1016/0004-6981(85)90167-2)
508 [6981\(85\)90167-2](https://doi.org/10.1016/0004-6981(85)90167-2), 1985.

509 Cousins, I. T., Dewitt, J. C., Glüge, J., Goldenman, G., Herzke, D., Lohmann, R., Ng, C. A.,
510 Scheringer, M. and Wang, Z.: The high persistence of PFAS is sufficient for their management
511 as a chemical class, *Environ Sci Process Impacts*, 22(12), 2307–2312, doi:[10.1039/d0em00355g](https://doi.org/10.1039/d0em00355g),
512 2020.

513 Crisp, T. A., Lerner, B. M., Williams, E. J., Quinn, P. K., Bates, T. S. and Bertram, T. H.:
514 Observations of gas phase hydrochloric acid in the polluted marine boundary layer, *J Geophys*
515 *Res*, (119), 6897–6915, doi:[10.1002/2013JD020992](https://doi.org/10.1002/2013JD020992), 2014.

516 Crosson, E. R.: A cavity ring-down analyzer for measuring atmospheric levels of methane,
517 carbon dioxide, and water vapor, *Appl Phys B Lasers Opt*, 92(3), 403–408, doi:[10.1007/s00340-](https://doi.org/10.1007/s00340-008-3135-y)
518 [008-3135-y](https://doi.org/10.1007/s00340-008-3135-y), 2008.

519 Dawe, K. E. R., Furlani, T. C., Kowal, S. F., Kahan, T. F., Vandenboer, T. C. and Young, C. J.:
520 Formation and emission of hydrogen chloride in indoor air, *Indoor Air*, 29, 70–78,
521 doi:[10.1111/ina.12509](https://doi.org/10.1111/ina.12509), 2019.

522 Deming, B. L., Pagonis, D., Liu, X., Day, D. A., Talukdar, R., Krechmer, J. E., Gouw, J. A. De,
523 Jimenez, J. L. and Ziemann, P. J.: Measurements of delays of gas-phase compounds in a wide
524 variety of tubing materials due to gas – wall interactions, , (1), 3453–3461, 2019.

525 ECHA: Four new substances added to Candidate List, 2020.

526 Eisele, F. L. and Tanner, D. J.: Measurement of the gas phase concentration of H₂SO₄ and
527 methane sulfonic acid and estimates of H₂SO₄ production and loss in the atmosphere, *J Geophys*
528 *Res Atmos*, 98(D5), 9001–9010, doi:[10.1029/93JD00031](https://doi.org/10.1029/93JD00031), 1993.

529 Ellis, R. a, Murphy, J. G., Pattey, E., Haarlem, R. Van and Brien, J. M. O.: Characterizing a
530 Quantum Cascade Tunable Infrared Laser Differential Absorption Spectrometer (QC-TILDAS
531) for measurements of atmospheric ammonia, *Atmos. Meas. Tech.*, 3309–3338, 2010.

532 Finlayson-Pitts, B. J., Ezell, M. J. and Pitts Jr., J. N.: Formation of chemically active chlorine
533 compounds by reactions of atmospheric NaCl particles with gaseous N₂O₅ and ClONO₂,
534 *Nature*, 337(6204), 241–244, 1989.

535 Furlani, T. C., Veres, P. R., Dawe, K. E. R., Neuman, J. A., Brown, S. S., VandenBoer, T. C. and
536 Young, C. J.: Gaseous HCl ambient intercomparison in Toronto Canada April 2019, *Fed Res*
537 *Data Repos*, doi:[10.20383/102.0486](https://doi.org/10.20383/102.0486), 2021.

538 Gard, E. E., Kleeman, M. J., Gross, D. S., Hughes, L. S., Allen, J. O., Morrical, B. D.,
539 Ferguson, D. P., Dienes, T., Ga, M. E., Johnson, R. J., Cass, G. R. and Prather, K. A.: Direct
540 Observation of Heterogeneous Chemistry in the Atmosphere, , 279(February), 1998.

541 Gordon, I. E., Rothman, L. S., Hill, C., Kochanov, R. V, Tan, Y., Bernath, P. F., Birk, M.,
542 Boudon, V., Campargue, A., Chance, K. V, Drouin, B. J., Flaud, J.-M., Gamache, R. R., Hodges,
543 J. T., Jacquemart, D., Perevalov, V. I., Perrin, A., Shine, K. P., Smith, M.-A. H., Tennyson, J.,
544 Toon, G. C., Tran, H., Tyuterev, V. G., Barbe, A., Császár, A. G., Devi, V. M., Furtenbacher, T.,
545 Harrison, J. J., Hartmann, J.-M., Jolly, A., Johnson, T. J., Karman, T., Kleiner, I., Kyuberis, A.

546 A., Loos, J., Lyulin, O. M., Massie, S. T., Mikhailenko, S. N., Moazzen-Ahmadi, N., Müller, H.
547 S. P., Naumenko, O. V, Nikitin, A. V, Polyansky, O. L., Rey, M., Rotger, M., Sharpe, S. W.,
548 Sung, K., Starikova, E., Tashkun, S. A., Auwera, J. Vander, Wagner, G., Wilzewski, J., Wcisło,
549 P., Yu, S. and Zak, E. J.: The HITRAN2016 molecular spectroscopic database, *J Quant*
550 *Spectrosc Radiat Transf*, 203, 3–69, doi:<https://doi.org/10.1016/j.jqsrt.2017.06.038>, 2017.

551 Hagen, C. L., Lee, B. C., Franka, I. S., Rath, J. L., Vandenboer, T. C., Roberts, J. M., Brown, S.
552 S. and Yalin, A. P.: Cavity ring-down spectroscopy sensor for detection of hydrogen chloride,
553 *Atmos Meas Tech*, 7(2), 345–357, doi:10.5194/amt-7-345-2014, 2014.

554 Haskins, J. D., Jaeglé, L., Shah, V., Lee, B. H., Lopez-Hilfiker, F. D., Campuzano-Jost, P.,
555 Schroder, J. C., Day, D. A., Guo, H., Sullivan, A. P., Weber, R., Dibb, J., Campos, T., Jimenez,
556 J. L., Brown, S. S. and Thornton, J. A.: Wintertime gas-particle partitioning and speciation of
557 inorganic chlorine in the lower troposphere over the northeast United States and coastal ocean, *J*
558 *Geophys Res Atmos*, 123(22), 12,897–12,916, doi:10.1029/2018JD028786, 2018.

559 Huey, L. G., Villalta, P. W., Dunlea, E. J., Hanson, D. R. and Howard, C. J.: Reactions of CF₃O-
560 with atmospheric trace gases, *J Phys Chem*, 100, 190–194, doi:10.1021/jp951928u, 1996.

561 Jurkat, T., Voigt, C., Arnold, F., Schlager, H., Aufmhoff, H., Schmale, J., Schneider, J.,
562 Lichtenstern, M. and Dörnbrack, A.: Airborne stratospheric ITCIMS measurements of SO₂, HCl,
563 and HNO₃ in the aged plume of volcano Kasatochi, *J Geophys Res Atmos*, 115(D2),
564 doi:<https://doi.org/10.1029/2010JD013890>, 2010.

565 Karellas, N. S., Chen, Q. F., De Brou, G. B. and Milburn, R. K.: Real time air monitoring of
566 hydrogen chloride and chlorine gas during a chemical fire, *J Hazard Mater*, 102(1), 105–120,
567 doi:[https://doi.org/10.1016/S0304-3894\(03\)00205-X](https://doi.org/10.1016/S0304-3894(03)00205-X), 2003.

568 Keene, W. C., Khalil, M. A. K., Erickson, D. J., McCulloch, A., Graedel, T. E., Lobert, J. M.,
569 Aucott, M. L., Gong, S. L., Harper, D. B., Kleiman, G., Midgley, P., Moore, R. M., Seuzaret, C.,
570 Sturges, W. T., Benkovitz, C. M., Koropalov, V., Barrie, L. A. and Li, Y. F.: Composite global
571 emissions of reactive chlorine from anthropogenic and natural sources: Reactive chlorine
572 emissions inventory, *J Geophys Res*, 104, 8429–8440, 1999.

573 Keene, W. C., Stutz, J., Pszenny, A. A. P., Maben, J. R., Fischer, E. V., Smith, A. M., von
574 Glasow, R., Pechtl, S., Sive, B. C. and Varner, R. K.: Inorganic chlorine and bromine in coastal
575 New England air during summer, *J Geophys Res Atmos*, 112(10), 1–15,
576 doi:10.1029/2006JD007689, 2007.

577 Keene, W. C., Long, M. S., Pszenny, A. A. P., Sander, R., Maben, J. R., Wall, A. J., O’Halloran,
578 T. L., Kerkweg, A., Fischer, E. V and Schrems, O.: Latitudinal variation in the multiphase
579 chemical processing of inorganic halogens and related species over the eastern North and South
580 Atlantic Oceans, *Atmos Chem Phys*, 9(19), 7361–7385, doi:10.5194/acp-9-7361-2009, 2009.

581 Kim, S., Huey, L. G., Stickel, R. E., Pierce, R. B., Chen, G., Avery, M. A., Dibb, J. E., Diskin,
582 G. S., Sachse, G. W., McNaughton, C. S., Clarke, A. D., Anderson, B. E. and Blake, D. R.:
583 Airborne Measurements of HCl from the Marine Boundary Layer to the Lower Stratosphere over
584 the North Pacific Ocean during INTEX-B, *Atmos. Chem. Phys. Discuss.*, 8, 3563–3595, 2008.

585 Kochanov, R. V, Gordon, I. E., Rothman, L. S., Shine, K. P., Sharpe, S. W., Johnson, T. J.,
586 Wallington, T. J., Harrison, J. J., Bernath, P. F., Birk, M., Wagner, G., Le Bris, K., Bravo, I. and

587 Hill, C.: Infrared absorption cross-sections in HITRAN2016 and beyond: Expansion for climate,
588 environment, and atmospheric applications, *J Quant Spectrosc Radiat Transf*, 230, 172–221,
589 doi:<https://doi.org/10.1016/j.jqsrt.2019.04.001>, 2019.

590 Lao, M., R. Crilley, L., Salehpoor, L., C. Furlani, T., Bourgeois, I., Andrew Neuman, J., W.
591 Rollins, A., R. Veres, P., A. Washenfelder, R., C. Womack, C., J. Young, C. and C. Vandenboer,
592 T.: A portable, robust, stable, and tunable calibration source for gas-phase nitrous acid (HONO),
593 *Atmos Meas Tech*, 13(11), 5873–5890, doi:10.5194/amt-13-5873-2020, 2020.

594 Lee, B. H., Lopez-Hilfiker, F. D., Schroder, J. C., Campuzano-Jost, P., Jimenez, J. L., McDuffie,
595 E. E., Fibiger, D. L., Veres, P. R., Brown, S. S., Campos, T. L., Weinheimer, A. J., Flocke, F. F.,
596 Norris, G., O'Mara, K., Green, J. R., Fiddler, M. N., Bililign, S., Shah, V., Jaeglé, L. and
597 Thornton, J. A.: Airborne Observations of Reactive Inorganic Chlorine and Bromine Species in
598 the Exhaust of Coal-Fired Power Plants, *J Geophys Res Atmos*, 123(19), 11,225–11,237,
599 doi:10.1029/2018JD029284, 2018.

600 Ma, Y., He, Y., Yu, X., Chen, C., Sun, R. and Tittel, F. K.: HCl ppb-level detection based on
601 QEPAS sensor using a low resonance frequency quartz tuning fork, *Sensors Actuators, B Chem*,
602 233, 388–393, doi:10.1016/j.snb.2016.04.114, 2016.

603 MacInnis, J. J., VandenBoer, T. C. and Young, C. J.: Development of a gas phase source for
604 perfluoroalkyl acids to examine atmospheric sampling methods, *Analyst*, 141, 3765–3775,
605 doi:10.1039/C6AN00313C, 2016.

606 Marcy, T. P., Fahey, D. W., Gao, R. S., Popp, P. J., Richard, E. C., Thompson, T. L., Rosenlof,
607 K. H., Ray, E. A., Salawitch, R. J., Atherton, C. S., Bergmann, D. J., Ridley, B. A., Weinheimer,
608 A. J., Loewenstein, M., Weinstock, E. M. and Mahoney, M. J.: Quantifying Stratospheric Ozone
609 in the Upper Troposphere with in Situ Measurements of HCl, *Science (80-)*, 304(5668), 261 LP
610 – 265, doi:10.1126/science.1093418, 2004.

611 Mattila, J. M., Lakey, P. S. J., Shiraiwa, M., Wang, C., Abbatt, J. P. D., Arata, C., Goldstein, A.
612 H., Ampollini, L., Katz, E. F., Decarlo, P. F., Zhou, S., Kahan, T. F., Cardoso-saldan, F. J., Ruiz,
613 L. H., Abeleira, A., Boedicker, E. K., Vance, M. E. and Farmer, D. K.: Multiphase chemistry
614 controls inorganic chlorinated and nitrogenated compounds in indoor air during bleach cleaning,
615 *Environ Sci Technol*, 54, 1730–1739, doi:10.1021/acs.est.9b05767, 2020.

616 Moravek, A., Singh, S., Pattey, E., Pelletier, L. and Murphy, J.: Measurements and quality
617 control of ammonia eddy covariance fluxes: a new strategy for high-frequency attenuation
618 correction, *Atmos Meas Tech*, 12, 6059–6078, doi:10.5194/amt-12-6059-2019, 2019.

619 Neuman, J. A., Huey, L. G., Ryerson, T. B. and Fahey, D. W.: Study of Inlet Materials for
620 Sampling Atmospheric Nitric Acid, *Environ Sci Technol*, 33(7), 1133–1136,
621 doi:10.1021/es980767f, 1999.

622 Osthoff, H. D., Roberts, J. M., Ravishankara, A. R., Williams, E. J., Lerner, B. M., Sommariva,
623 R., Bates, T. S., Coffman, D., Quinn, P. K., Dibb, J. E., Stark, H., Burkholder, J. B., Talukdar, R.
624 K., Meagher, J., Fehsenfeld, F. C. and Brown, S. S.: High levels of nitryl chloride in the polluted
625 subtropical marine boundary layer, *Nat Geosci*, 1(5), 324–328, 2008.

626 Pagonis, D., Krechmer, J. E., de Gouw, J., Jimenez, J. L. and Ziemann, P. J.: Effects of gas-wall
627 partitioning in Teflon tubing and instrumentation on time-resolved measurements of gas-phase

628 organic compounds, *Atmos. Meas. Tech.*, 10(12), 4687–4696, doi:10.5194/amt-10-4687-2017,
629 2017.

630 Place, B. K., Young, C. J., Ziegler, S. E., Edwards, K. A., Salehpoor, L. and VandenBoer, T. C.:
631 Passive sampling capabilities for ultra-trace quantitation of atmospheric nitric acid (HNO₃) in
632 remote environments, *Atmos Environ*, 191(November 2017), 360–369,
633 doi:10.1016/j.atmosenv.2018.08.030, 2018.

634 Pollack, I. B., Lindaas, J., Roscioli, J. R., Agnese, M., Permar, W., Hu, L. and Fischer, E. V:
635 Evaluation of ambient ammonia measurements from a research aircraft using a closed-path QC-
636 TILDAS operated with active continuous passivation, *Atmos. Meas. Tech.*, 12(7), 3717–3742,
637 doi:10.5194/amt-12-3717-2019, 2019.

638 Pszenny, A. A. P., Keene, W. C., Jacob, D. J., Fan, S., Maben, J. R., Zetwo, M. P., Springer-
639 Young, M. and Galloway, J. N.: Evidence of inorganic chlorine gases other than hydrogen
640 chloride in marine surface air, *Geophys Res Lett*, 20(8), 699–702, 1993.

641 Roberts, J. M., Osthoff, H. D., Brown, S. S. and Ravishankara, A. R.: N₂O₅ oxidizes chloride to
642 Cl₂ in acidic atmospheric aerosol, *Science* (80-), 321(4), 10, 2008.

643 Roscioli, J. R., Zahniser, M. S., Nelson, D. D., Herndon, S. C. and Kolb, C. E.: New Approaches
644 to Measuring Sticky Molecules: Improvement of Instrumental Response Times Using Active
645 Passivation, *J Phys Chem A*, 120(9), 1347–1357, doi:10.1021/acs.jpca.5b04395, 2016.

646 Sherwen, T., Schmidt, J. A., Evans, M. J., Carpenter, L. J., Großmann, K., Eastham, S. D., Jacob,
647 D. J., Dix, B., Koenig, T. K., Sinreich, R., Ortega, I., Volkamer, R., Saiz-Lopez, A., Prados-
648 Roman, C., Mahajan, A. S. and Ordóñez, C.: Global impacts of tropospheric halogens (Cl, Br, I)
649 on oxidants and composition in GEOS-Chem, *Atmos. Chem. Phys.*, 16(18), 12239–12271,
650 doi:10.5194/acp-16-12239-2016, 2016.

651 Simpson, W. R., Glasow, R. Von, Riedel, K., Anderson, P., Ariya, P., Bottenheim, J., Burrows,
652 J. and Carpenter, L. J.: Halogens and their role in polar boundary-layer ozone depletion, *Atmos*
653 *Chem Phys*, 4375–4418, 2007.

654 Simpson, W. R., Brown, S. S., Saiz-Lopez, A., Thornton, J. A. and Von Glasow, R.:
655 Tropospheric halogen chemistry: Sources, cycling, and impacts, *Chem Rev*, 115(10), 4035–
656 4062, doi:10.1021/cr5006638, 2015.

657 Sintermann, J., Spirig, C., Jordan, A., Kuhn, U., Ammann, C. and Neftel, A.: Eddy covariance
658 flux measurements of ammonia by high temperature chemical ionisation mass spectrometry,
659 *Atmos. Meas. Tech.*, 4(3), 599–616, doi:10.5194/amt-4-599-2011, 2011.

660 Solomon, S.: Stratospheric ozone depletion: A review of concepts and history, *Rev Geophys*,
661 37(3), 275–316, doi:10.1029/1999RG900008, 1999.

662 Sunderland, E. M., Hu, X. C., Dassuncao, C., Tokranov, A. K., Wagner, C. C. and Allen, J. G.:
663 A review of the pathways of human exposure to poly- and perfluoroalkyl substances (PFASs)
664 and present understanding of health effects, *J Expo Sci Environ Epidemiol*, 29(2), 131–147,
665 doi:10.1038/s41370-018-0094-1, 2019.

666 Thaler, R. D., Mielke, L. H. and Osthoff, H. D.: Quantification of Nitryl Chloride at Part Per
667 Trillion Mixing Ratios by Thermal Dissociation Cavity Ring-Down Spectroscopy, *Anal Chem*,

668 83(7), 2761–2766, doi:10.1021/ac200055z, 2011.

669 Thornton, J. A., Kercher, J. P., Riedel, T. P., Wagner, N. L., Cozic, J., Holloway, J. S., Dube, W.
670 P., Wolfe, G. M., Quinn, P. K., Middlebrook, A. M., Alexander, B. and Brown, S. S.: A large
671 atomic chlorine source inferred from mid-continental reactive nitrogen chemistry, *Nature*,
672 464(11), 271–274, doi:10.1038/nature08905, 2010.

673 United States Environmental Protection Agency: Compendium of Methods for the Determination
674 of Inorganic Compounds in Ambient Air: Determination of reactive acidic and basic gases and
675 strong acidity of atmospheric fine particles (<2.5 μm) (Compendium Method IO-4.2)., 1999.

676 Valach, R.: The origin of the gaseous form of natural atmospheric chlorine ', *Tellus Ser B Chem*
677 *Phys Meteorol*, 1967.

678 Veres, P. R., Roberts, J. M., Warneke, C., Welsh-Bon, D., Zahniser, M., Herndon, S., Fall, R.
679 and de Gouw, J.: Development of negative-ion proton-transfer chemical-ionization mass
680 spectrometry (NI-PT-CIMS) for the measurement of gas-phase organic acids in the atmosphere,
681 *Int J Mass Spectrom*, 274, 48–55, 2008.

682 Voss, P. B., Stimpfle, R. M., Cohen, R. C., Hanisco, T. F., Bonne, G. P., Perkins, K. K.,
683 Lanzendorf, E. J., Anderson, J. G., Salawitch, R. J., Webster, C. R., Scott, D. C., May, R. D.,
684 Wennberg, P. O., Newman, P. A., Lait, L. R., Elkins, J. W. and Bui, T. P.: Inorganic chlorine
685 partitioning in the summer lower stratosphere: Modeled and measured $[\text{ClONO}_2]/[\text{HCl}]$ during
686 POLARIS, *J Geophys Res Atmos*, 106(D2), 1713–1732,
687 doi:<https://doi.org/10.1029/2000JD900494>, 2001.

688 Wang, X., Jacob, D. J., Eastham, S. D., Sulprizio, M. P., Zhu, L., Chen, Q., Alexander, B.,
689 Sherwen, T., Evans, M. J., Lee, B. H., Haskins, J. D., Lopez-Hilfiker, F. D., Thornton, J. A.,
690 Huey, G. L. and Liao, H.: The role of chlorine in global tropospheric chemistry, *Atmos Chem*
691 *Phys*, 19(6), 3981–4003, doi:10.5194/acp-19-3981-2019, 2019.

692 Webster, C. R., May, R. D., Trimble, C. A., Chave, R. G. and Kendall, J.: Aircraft (ER-2) laser
693 infrared absorption spectrometer (ALIAS) for in-situ stratospheric measurements of HCl, N₂O,
694 CH₄, NO₂, and HNO₃, *Appl Opt*, 33(3), 454–472, doi:10.1364/AO.33.000454, 1994.

695 Whitehead, J. D., Twigg, M., Famulari, D., Nemitz, E., Sutton, M. A., Gallagher, M. W. and
696 Fowler, D.: Evaluation of Laser Absorption Spectroscopic Techniques for Eddy Covariance Flux
697 Measurements of Ammonia, *Environ Sci Technol*, 42(6), 2041–2046, doi:10.1021/es071596u,
698 2008.

699 Wilkerson, J., Sayres, D., Smith, J., Allen, N., Rivero, M., Greenberg, M., Martin, T. and
700 Anderson, J.: In situ observations of stratospheric HCl using three-mirror integrated cavity
701 output spectroscopy, *Atmos Meas Tech*, 14(5), 3597–3613, doi:10.5194/amt-14-3597-2021,
702 2021.

703 Young, A. H., Keene, W. C., Pszenny, A. A. P., Sander, R., Thornton, J. A., Riedel, T. P. and
704 Maben, J. R.: Phase partitioning of soluble trace gases with size-resolved aerosols in near-surface
705 continental air over northern Colorado, USA, during winter, *J Geophys Res*, 118, 9414–9427,
706 doi:10.1002/jgrd.50655, 2013.

707 Young, C. J., Washenfelder, R. A., Roberts, J. M., Mielke, L. H., Osthoff, H. D., Tsai, C.,

708 Pikelnaya, O., Stutz, J., Veres, P. R., Cochran, A. K., Vandenkoer, T. C., Flynn, J., Grossberg,
709 N., Haman, C. L., Lefer, B., Stark, H., Graus, M., De Gouw, J., Gilman, J. B., Kuster, W. C. and
710 Brown, S. S.: Vertically resolved measurements of nighttime radical reservoirs in los angeles and
711 their contribution to the urban radical budget, *Environ Sci Technol*, 46(20),
712 doi:10.1021/es302206a, 2012.

713 Young, C. J., Washenfelder, R. A., Edwards, P. M., Parrish, D. D., Gilman, J. B., Kuster, W. C.,
714 Mielke, L. H., Osthoff, H. D., Tsai, C., Pikelnaya, O., Stutz, J., Veres, P. R., Roberts, J. M.,
715 Griffith, S., Dusanter, S., Stevens, P. S., Flynn, J., Grossberg, N., Lefer, B., Holloway, J. S.,
716 Peischl, J., Ryerson, T. B., Atlas, E. L., Blake, D. R. and Brown, S. S.: Chlorine as a primary
717 radical: evaluation of methods to understand its role in initiation of oxidative cycles, *Atmos*
718 *Chem Phys*, 14, 3427–3440, 2014.

719 Young, C. J., Zhou, S., Siegel, J. A. and Kahan, T. F.: Illuminating the dark side of indoor
720 oxidants, *Environ Sci Process Impacts*, 21(8), 1229–1239, doi:10.1039/C9EM00111E, 2019.

721 Zahniser, M. S., Nelson, D. D., McManus, B., Keabian, P. L., Lloyd, D., Fowler, D., Jenkinson,
722 D. S., Monteith, J. L. and Unsworth, M. H.: Measurement of trace gas fluxes using tunable diode
723 laser spectroscopy, *Philos Trans R Soc London Ser A Phys Eng Sci*, 351(1696), 371–382,
724 doi:10.1098/rsta.1995.0040, 1995.

725